6 Charge Self-Consistency in Correlated Electronic Structure Calculations

Frank Lechermann
I. Institut für Theoretische Physik
Universität Hamburg
Jungiusstraße 9, 20355 Hamburg

Contents

E. Pavarini, E. Koch, A. Lichtenstein, and D. Vollhardt (eds.)
DMFT: From Infinite Dimensions to Real Materials
Modeling and Simulation Vol. 8
Forschungszentrum Jülich, 2018, ISBN 978-3-95806-313-6
http://www.cond-mat.de/events/correl18

1 Introduction

The last twenty years have witnessed extraordinary progress in the theoretical description and modeling of so-called strongly correlated materials. In these realistic condensed matter systems, the screening of the Coulomb interaction between electrons is too weak to rely on effective single-particle approaches. The electron-electron interaction becomes a natural competitor of the basic hopping processes, thus intriguing electronic many-body instabilities characterized by different degrees of itinerancy and localization occur.

The combination of density-functional theory (DFT) with dynamical mean-field theory (DMFT) emerged as a major approach to tackle the challenges of strongly correlated systems on a realistic level. Metal-insulator transitions, local-moment formation, spin and charge fluctuations, finite-temperature effects on correlated electron states, or the interplay of correlations with spin-orbit coupling are only a few hallmark topics that have been studied successfully with the so-called DFT+DMFT scheme. As a hybrid method, interfacing band theory and quantum chemistry for demanding condensed-matter problems, the basic formalism is delicate. In this chapter, the goal is to shed light on the specific aspect of "self-consistency" in numerical accounts of the correlated electronic structure of materials. Though there are various techniques where this issue applies, in order to keep the discussion straight and within reasonable length, the main body of this treatise will focus on the matter within DFT+DMFT, which is nowadays the key method for *strongly* correlated materials.

Briefly, in basic mathematical terms, *self-consistency* is figured as the both-way matching of an implicit defining function, e.g., a potential $v(\mathbf{r})$, with a depending function, e.g., a wave function $\psi(\mathbf{r})$, that are related by a set of (partial) differential equations derived from a variational treatment of the (free) energy of the system. Since such a set of equations is usually not solvable by analytical means, a numerical solution may be reached iteratively. Starting from some reasonable initial guess, consecutive constructions of ψ_v and v_ψ will eventually result in a *self-consistent solution* for $\{v(\mathbf{r}), \psi(\mathbf{r})\}$ subject to the governing set of equations. Note that there are also still other kinds of (self-)consistencies in iterative mathematical equations, such as, e.g., for the Verhulst equation. In the DFT+DMFT context, and depending on how this approach is put into practice, we will encounter different situations of self-consistency of the given kind. Among those, *charge self-consistency* plays a singular role, as it closes the calculational iteration loop (in the sense sketched above) of the complete scheme on the outermost level.

In the present scope, charge self-consistency is attributed to a necessary incoherent theoretical description of an electronic system. In the simplest manner, one imagines the whole system being divided into two subsystems which are treated by a different degree of sophistication. Then, charge self-consistency holds if three features are installed:

1. Exchange of charge between the two subsystems is possible.
2. Even without explicit charge flow inbetween, the electronic structure within one subsystem (i.e., its field) affects the electronic structure in the other subsystem (and vice versa).
3. The combined theoretical scheme as a whole is self-consistent in the sense that the complete electronic structure is at a stationary point of the thermodynamics.

Although investigations without charge self-consistency may often provide already valuable insight into the physics of correlated materials, it turns out that in several important cases this form of self-consistency does not only matter by quantitative means. Qualitative differences, e.g., wether a given compound is Mott insulating or not, do occur.
The text is organized as follows. In section 2 the basic forms of self-consistency in the original Hartree-Fock method as well as in pure DFT and pure DMFT will be reviewed to set the stage. Section 3 then deals with a description of the DFT+DMFT approach, both on a formal and on a practical level. Emphasis will be put on the latter, especially on the relevance of the charge self-consistent aspect. To illustrate the presented theoretical concepts at work, a concrete materials examples is discussed in the final section 4.

2 Self-consistency in numerical approaches to many-electron systems

In order to get acquainted with the basic ideas and mechanisms of self-consistency problems in advanced quantum mechanics, let us first start with a condensed reminder of the canonical schemes of computational many-body theory for electronic systems. As for the complete rest of the paper, we will remain within the Born-Oppenheimer approximation of separating electronic and ionic degrees of freedom, focussing on the former one. Furthermore, we remain in the nonrelativistic regime, hence exclude, e.g., spin-orbit effects to keep the discussion elementary. Three different key observables will be discussed, namely the many-body wave function $\Psi(\{\mathbf{r}\sigma\})$ in the context of Hartree-Fock, the electronic charge density $\rho(\mathbf{r})$ in the context of DFT and the one-particle Green function $G(\mathbf{k},\omega)$ in the context of DMFT.

2.1 Hartree-Fock method

The Hartree-Fock (HF) method (see e.g. Ref. [1] for a review) is routed in quantum chemistry, providing basic access to the electronic system of atoms and molecules with N electrons. It serves as the starting point for more involved approaches such as, e.g., Møller-Plesset theory or the configuration-interaction scheme.
Key idea is the ansatz for the many-body wave function $\Psi(\{\mathbf{r}_i\sigma_i\}) =: \Psi(\{\mathbf{x}_i\})$ as a single Slater determinant , i.e.

$$\Psi_{\mathrm{HF}}(\{\mathbf{x}_i\}) =: \hat{S}_- \prod_i^N \varphi_i(\mathbf{r})\chi_i(\sigma) = \hat{S}_- \prod_i^N \phi_i(\mathbf{x}) \quad , \quad \text{with} \qquad \varphi_i(\mathbf{r}) = \sum_\nu^M A_{i\nu}\, B_\nu(\mathbf{r}) \; . \quad (1)$$

Here, $\hat{S}_-$ is the antisymmetrization operator, φ the real-space function, χ the spin function and $i = 1, N$. The functions φ_i are expanded into M basis functions B_ν, usually of atomic kind, with expansion coefficients $A_{i\nu}$. In the end, the $A_{i\nu}$ are the parameters that will be optimized for the solution. It is very important to realize that the ansatz (1) marks the *simplest possible* wave function for an electronic system, describing independent electrons only subject to the

Pauli exclusion principle. The Hamiltonian of the electronic system with momenta p_i and the potential V_i of the nuclei is straightforwardly written as

$$\hat{H} = \sum_i^N \left(\frac{\hat{p}_i^2}{2m} + \hat{V}_i \right) + \frac{1}{2} \sum_{ij} \hat{v}_{ij} =: \sum_i^N \hat{h}_i + \frac{1}{2} \sum_{ij} \hat{v}_{ij} \; . \tag{2}$$

The two-particle operator $\hat{v}_{ij}$ represents the Coulomb interaction between the electrons. To obtain a working scheme for the optimization of our trial wave function with regard to the given problem, we make use of the Ritz variational principle

$$\delta \left(\frac{\langle \Psi_{\rm HF} | \hat{H} | \Psi_{\rm HF} \rangle}{\langle \Psi_{\rm HF} | \Psi_{\rm HF} \rangle} \right) \stackrel{!}{=} 0 \, , \tag{3}$$

with the relevant expectation value reading

$$\langle \Psi_{\rm HF} | \hat{H} | \Psi_{\rm HF} \rangle = \sum_i \langle \phi_i | \hat{h} | \phi_i \rangle + \frac{1}{2} \sum_{ij} \Big(\underbrace{\langle \phi_j \phi_i | \hat{v} | \phi_j \phi_i \rangle}_{\text{Coulomb (Hartree) term}} - \underbrace{\langle \phi_j \phi_i | \hat{v} | \phi_i \phi_j \rangle}_{\text{exchange (Fock) term}} \Big), \tag{4}$$

and the corresponding real-space matrix elements

$$\langle \phi_i | \hat{h} | \phi_i \rangle = \int d\mathbf{r} \, \varphi_i^*(\mathbf{r}) \, h(\mathbf{r}) \, \varphi_i(\mathbf{r}) \, , \tag{5}$$

$$\langle \phi_i \phi_j | \hat{v} | \phi_k \phi_l \rangle = \delta_{\sigma_i \sigma_k} \delta_{\sigma_j \sigma_l} \int d\mathbf{r} d\mathbf{r}' \, \varphi_i^*(\mathbf{r}) \varphi_j^*(\mathbf{r}') \, v(\mathbf{r}, \mathbf{r}') \, \varphi_k(\mathbf{r}) \varphi_l(\mathbf{r}') \, . \tag{6}$$

Note that the general Coulomb matrix element is spin dependent, though the interaction surely is not. The reason is the enforcement of the Pauli principle in electron-electron scattering process. The Ritz principle is most effectively put into practice via minimizing the functional form

$$\mathcal{F}[\Psi_{\rm HF}] = \langle \Psi_{\rm HF} | \hat{H} | \Psi_{\rm HF} \rangle - \sum_i \varepsilon_i \langle \phi_i | \phi_i \rangle \quad , \text{ with} \qquad \delta \mathcal{F} \stackrel{!}{=} 0 \, , \tag{7}$$

whereby the ε_i serve as lagrange multipliers. The variation implies here a functional differentiation with $\phi_i \to \phi_i + \delta \phi_i$. This leads to the single-particle or *Hartree-Fock equations* governed by the so-called Fock operator $\hat{F}$, i.e.

$$\hat{F} \, | \phi_i \rangle = \varepsilon_i \, | \phi_i \rangle \qquad \forall \, i \tag{8}$$

and are written in real-space representation as ($\hbar = 1$)

$$\left(-\frac{1}{2m} \Delta + V(\mathbf{r}) + e^2 \sum_{j \neq i} \int d\mathbf{r}' \, \frac{|\varphi_j(\mathbf{r})|^2}{|\mathbf{r} - \mathbf{r}'|} \right) \phi_i(\mathbf{r}) - e^2 \sum_{j \neq i} \delta_{\sigma_i \sigma_j} \int d\mathbf{r}' \, \frac{\varphi_j^*(\mathbf{r}) \varphi_i^*(\mathbf{r}')}{|\mathbf{r} - \mathbf{r}'|} \phi_j(\mathbf{x}) = \varepsilon_i \phi_i(\mathbf{x}) \tag{9}$$

$$\Rightarrow \quad \left(-\frac{1}{2m} \Delta + V(\mathbf{r}) + v_{\rm H}(\mathbf{r}) \right) \varphi_i(\mathbf{r}) + \int d\mathbf{r}' \, v_{\rm X}(\mathbf{r}, \mathbf{r}') \, \varphi_i(\mathbf{r}) = \varepsilon_i \varphi_i(\mathbf{r}) \, . \tag{10}$$

The local Hartree potential $v_{\rm H}(\mathbf{r})$ describes the Coulomb repulsion between electrons, as familiar from classical electrostatics. The nonlocal exchange potential $v_{\rm X}(\mathbf{r}, \mathbf{r}')$ adds unique quantum

physics due to the Pauli principle: electrons with equal spin effectively feel a repelling potential to avoid each other not to join a common quantum state. Note already here that, in a quantum-chemistry definition, there is still a third mechanism, also of pure quantum kind, that influences the concerted arrangement among the electrons. It is called *correlation*, not directly related to spin, and goes beyond the Hartree-Fock picture, since it is encrypted in more complicated many-electron wave functions than the most simple one of single Slater-determinant kind. It is thus very important for the understanding of the Hartree-Fock equations to appreciate the ansatz (1) that lead to eq. (10).

For us here, the principle solution of the Schrödinger-like eq. (10) is the main concern. It becomes clear from (9) that contrary to the standard nuclear potential $V(\mathbf{r})$, the Hartree and exchange potential are not given from the beginning. They explicitly dependent on the wave functions φ_i we are actually looking for. Therefore, the implicit character of the Hartree-Fock equations forms a natural *self-consistency* problem. In the literature, these equations are thus also often termed *self-consistent field (SCF)* equations. Literally, the solution is defined by an iterative cycle as follows:

1. Start with an educated guess for the single-particle functions $\varphi_i(\mathbf{r}) = \varphi_i^{(1)}(\mathbf{r})$ by invoking suitable linear combinations of the basis functions. For instance, an adequate kind of sp^n hybridization function might be meaningful for a carbon-based molecule.
2. Construct a first associated Hartree potential $v_{\mathrm{H}}^{(1)}(\mathbf{r}) = v_{\mathrm{H}}^{\{\varphi_i^{(1)}\}}(\mathbf{r})$ and exchange potential $v_{\mathrm{X}}^{(1)}(\mathbf{r}) = v_{\mathrm{X}}^{\{\varphi_i^{(1)}\}}(\mathbf{r}, \mathbf{r}')$ and solve the Hartree-Fock equations for a new set of eigenfunctions $\varphi_i^{(2)}(\mathbf{r})$.
3. Go back to step 2 and repeat p times until you reach convergence in the potentials, i.e., $|v_{\mathrm{H}}^{(p)} - v_{\mathrm{H}}^{(p-1)}| < \eta$ and $|v_{\mathrm{X}}^{(p)} - v_{\mathrm{X}}^{(p-1)}| < \eta$ holds for small η.

We will remark in section 2.4 on further relevant technical aspects of performing this self-consistency cycle. If this cycle converges, it is obvious for us physicists that the resulting functions $\varphi_i^{(p)}$ along with their eigenvalues $\varepsilon_i^{(p)}$ represent a faithful solution to the problem. A *principle* convergence is ensured by the variational character of how we casted the problem. But note that in general, such self-consistency problems can underlie the issues of local vs. global minimum, existence of saddle-points, etc.. In this text however, we will not delve into these mathematical aspects of the solution space.

We have now encountered a first concrete self-consistency problem for many-electron systems. This Hartree-Fock method obviously may also be termed a *charge self-consistent method*, as the electronic charge density $\rho(\mathbf{r})$ is implicitly also iterated in the cycle given above and can be expressed via a sum over the occupied orbitals

$$\rho(\mathbf{r}) = \sum_{i}^{\mathrm{occ}} |\varphi_i(\mathbf{r})|^2 \,. \tag{11}$$

Thus the charge distribution always matches the associated electron states and also the total charge is conserved. By this statement, we have assumed that *all* electrons of the system enter

in eq. (10). If instead, one decides to, e.g., "freeze" some core electrons in their atomic state and to only Hartree-Fock converge chosen valence electrons, then complete charge self-consistency would in principle not be achieved. Neither valence nor core charge density would be in accordance with the distribution at the global stability point of the system. Further relaxation of the core states could still modify the charge density of the whole system.
We leave the further analysis of the Hartree-Fock solution as well as the description of the plethora of different method flavors to the numerous textbooks on this matter, and continue by an theory advancement that builds up directly on the electronic charge density $\rho(\mathbf{r})$.

2.2 Density-functional theory (DFT) in Kohn-Sham representation

Besides the obvious flaw of Hartree-Fock in missing the effect of *correlation*, there are further serious drawbacks. The scheme is ill-defined for crystalline systems and the nonlocal exchange potential is computationally delicate and expensive. Instead of working directly with a many-body wave function $\Psi(\{\mathbf{x}_i\})$, it appears also more attractive to deal with a physically more tangible object.
Density-functional theory (DFT) puts the electronic charge density $\rho(\mathbf{r})$ in the focus and has become the workhorse of quantum-mechanical calculations for materials since more than thirty years (see e.g. Refs. [2, 3] for reviews). It builds upon the theorems by Hohenberg and Kohn, stating, in short, first that $\rho(\mathbf{r})$ bears *in principle* the same physically-relevant information as the much more complex $\Psi(\{\mathbf{x}_i\})$. Second, the functional $E[\rho]$ of the system's total energy has a minimum for the correct ground state charge density $\rho_0(\mathbf{r})$, thus ensuring a variational principle. Equipped with the already gathered knowledge, we may cast such a functional straightforwardly (by adjusting to the community-established nomenclature) in the form

$$E[\rho] = T[\rho] + \int d\mathbf{r}\, \rho(\mathbf{r}) v_{\rm ext}(\mathbf{r}) + E_{\rm H}[\rho] + E_{\rm QMB}[\rho]\ . \tag{12}$$

The kinetic-energy contribution is denoted $T[\rho]$, $v_{\rm ext}(\mathbf{r})$ is nothing but the former nuclear potential $V(\mathbf{r})$ and $E_{\rm H}[\rho]$ describes the Hartree energy. All the remaining (and notorious) explicit quantum many-body terms, namely the effect of Pauli principle and correlation, enter the functional $E_{\rm QMB}[\rho]$. The expression (12) is also important because of its hierarchical structure: in direct comparison, all but the term $E_{\rm QMB}$ are reasonably large.
To proceed towards a practical formalism, one invokes in the so-called *Kohn-Sham (KS) representation* of DFT a virtual non-interacting electron system [4]. Such a system is surely exactly represented by a single Slater determinant. As a key step, we demand that the electronic charge density, and then obviously also the total energy, of the real system and the virtual system coincide. This means that in our virtual system, there must be a rather tricky effective potential $v_{\rm KS}(r)$ at work that enforces this demand. It is hence natural to continue as follows

$$E[\rho] \stackrel{!}{=} E_{\rm virt.\,sys.}[\rho] \ := \ T_{\rm S}[\rho] + \int d\mathbf{r}\, \rho(\mathbf{r}) v_{\rm KS}(\mathbf{r}) \tag{13}$$

$$= \ T_{\rm S}[\rho] + \int d\mathbf{r}\, \rho(\mathbf{r}) v_{\rm ext}(\mathbf{r}) + \frac{e^2}{2} \int d\mathbf{r} d\mathbf{r}'\, \frac{\rho(\mathbf{r})\rho(\mathbf{r}')}{|\mathbf{r}-\mathbf{r}'|} + E_{\rm xc}[\rho]\ . \tag{14}$$

Equation (14) again establishes an educated guess based on what we learned from embarking on Hartree-Fock theory. The total energy has to consist of four terms: a kinetic energy $T_{\rm S}$ now of non-interacting electrons, an electron-nuclear interaction, a classical Hartree term, and last but not least a term that includes the quantum many-body terms, here named $E_{\rm xc}$. Note that the latter *exchange-correlation functional* does not only include the effect of Pauli exchange and correlation, but also the difference $T-T_S$ from implicit quantum many-body effects in the kinetic energy.

Why should the form (14) be preferred over the expression (12)? Because (14) is amenable to straightforward numerical treatment. Since deep down there may be only single-particle wave functions that build up the expression (14), we can immediately formulate the according variational principle

$$\delta \left(E[n] - \sum_i \varepsilon_i \langle \varphi_i | \varphi_i \rangle \right) \stackrel{!}{=} 0 \,, \tag{15}$$

leading to the so-called *Kohn-Sham equations*

$$\left(-\frac{1}{2m} \Delta + v_{\rm KS}(\mathbf{r}) \right) \varphi_i(\mathbf{r}) = \varepsilon_i \, \varphi(\mathbf{r}) \tag{16}$$

of effective-single-particle kind. Accordingly, the effective, or KS, potential reads

$$v_{\rm KS}(\mathbf{r}) = v_{\rm ext}(\mathbf{r}) + v_{\rm H}(\mathbf{r}) + v_{\rm xc}(\mathbf{r}), \text{ with } \quad v_{\rm xc}(\mathbf{r}) = \frac{\delta E_{\rm xc}}{\delta \rho} \,. \tag{17}$$

In practice, the total energy is usually computed via expressing the kinetic-energy term through the eigenvalue sum, resulting in

$$E_{\rm DFT} = \sum_i \varepsilon_i - \frac{e^2}{2} \int d\mathbf{r} d\mathbf{r}' \, \frac{\rho(\mathbf{r}) \rho(\mathbf{r}')}{|\mathbf{r} - \mathbf{r}'|} - \int d\mathbf{r} \, \rho(\mathbf{r}) v_{\rm xc}(\mathbf{r}) + E_{\rm xc}[\rho] \,. \tag{18}$$

It is clear that the exchange-correlation part asks for approximations. Originally, reference to a numerically-exact quantum Monte-Carlo treatment of the homogeneous electron gas is made and the exchange-correlation energy (in fact, the correlation part, since the exchange part is analytically known) extracted via an analytical fit $\epsilon_{\rm xc}(\rho)$. The resulting ansatz

$$E_{\rm xc}[\rho] = \int d\mathbf{r} \, \rho(\mathbf{r}) \epsilon_{\rm xc}(\rho(\mathbf{r})) \tag{19}$$

defines the so-called *local-density approximation (LDA)* . Further approximations for $E_{\rm xc}[\rho]$, such as the generalized gradient approximation (GGA) which includes gradient terms of the charge density, exist. Finally, the electronic charge density is again expressed by the sum over the occupied effective single-particle states, i.e., of form (11). The careful reader may have noted that we did not include the spin degree of freedom by explicit means in our argumentation. This is due to the fact that in *exact* DFT, this degree of freedom is not of evident relevance, as an exact exchange-correlation functional incorporates the effect of spin. In practical and eventually approximate Kohn-Sham representation, eq. (16) gains a spin index describing spin-up and spin-down charge densities and the canonical xc-approximation is the local spin-density approximation (LSDA).

It is obvious from eqns. (16) and (17) that the practical Kohn-Sham scheme is again based on a self-consistency cycle similar to that described for the Hartree-Fock method. Here, the local Kohn-Sham potential $v_{\rm KS}(\mathbf{r})$ has to be iterated until convergence. Charge self-consistency is naturally ensured in KS calculations, although in principle, also here a possibly different treatment of, e.g., core and valence electrons would abandon an exact charge self-consistent state. Such differences indeed occur in various KS-based electronic structure codes of, e.g., selected augmented-wave or pseudopotential kind. However, the differences in the total charge density (especially in the relevant spatial regions) are very small and the resulting physics of interest is not affected. Thus for the rest of these notes, KS-based DFT is understood as a charge self-consistent framework.
Especially for solid-state system, Kohn-Sham calculations greatly improve on Hartree-Fock studies, since the reasonable treatment of the exchange and correlation within LDA enables the important description of screening of the Coulomb potential. For further aspects of density-functional theory and the Kohn-Sham representation we refer to the various excellent reviews. In the following, to simplify the writing, it is understood that "DFT" refers to the KS-representation of density-functional theory.

2.3 Dynamical mean-field theory (DMFT)

In terms of electronic correlations, we advanced from no consideration at all in Hartree-Fock to a reasonably-well treatment for many materials within DFT. Still, for some materials classes, e.g., transition-metal oxides, the DFT description of the correlated behavior of electrons remains insufficient. Most notably, in these systems the delicate competition among electrons between itinerancy and the tendency to localize in real space asks for a better modeling. The dynamical mean-field theory (DMFT) [5,6] is a hallmark condensed-matter framework that faces this task best for such *strongly correlated materials*. It utilizes the one-particle Green function as key to provide seminal access to the spectral properties and the total energy of an interacting electron system on a lattice, and was originally constructed in a model-Hamiltonian context.
Contrary to Hartree-Fock and original DFT, the DMFT approach is designed to work at finite temperature T. Hence we introduce fermionic Matsubara frequencies $\omega_{\rm n} := (2n+1)\pi T$ to write the correct Green function for the Hamiltonian $H(\mathbf{k})$ at wave vector $\mathbf{k}$ in reciprocal space as

$$G(\mathbf{k}, i\omega_{\rm n}) = \big(i\omega_{\rm n} + \mu - H(\mathbf{k}) - \Sigma(\mathbf{k}, i\omega_{\rm n})\big)^{-1}, \tag{20}$$

whereby μ is the chemical potential and $\Sigma(\mathbf{k}, i\omega_{\rm n})$ the so-called *self-energy* of the system. Expression (20) looks quite different from the electronic-state descriptions we encountered so far. But the Green function formalism is just a different *representation* of the physics, especially tailored to systems with sizable correlations in the solid state. For instance, we could also easily express the Hartree-Fock or DFT pictures therein, namely via the according self-energies

$$\Sigma_{\rm HF}(\mathbf{k}, i\omega_n) = \sum_{\mathbf{q}} (v_{\mathbf{kqkq}} - v_{\mathbf{qkkq}}) \left(\mathrm{e}^{\beta(\varepsilon_{\mathbf{q}}-\mu)} + 1\right)^{-1}, \tag{21}$$

$$\Sigma_{\rm DFT}(\mathbf{k}, i\omega_n) = \sum_{\mathbf{q}} (v_{\rm H} + v_{\rm xc})_{\mathbf{kqkq}} \left(\mathrm{e}^{\beta(\varepsilon_{\mathbf{q}}-\mu)} + 1\right)^{-1}, \tag{22}$$

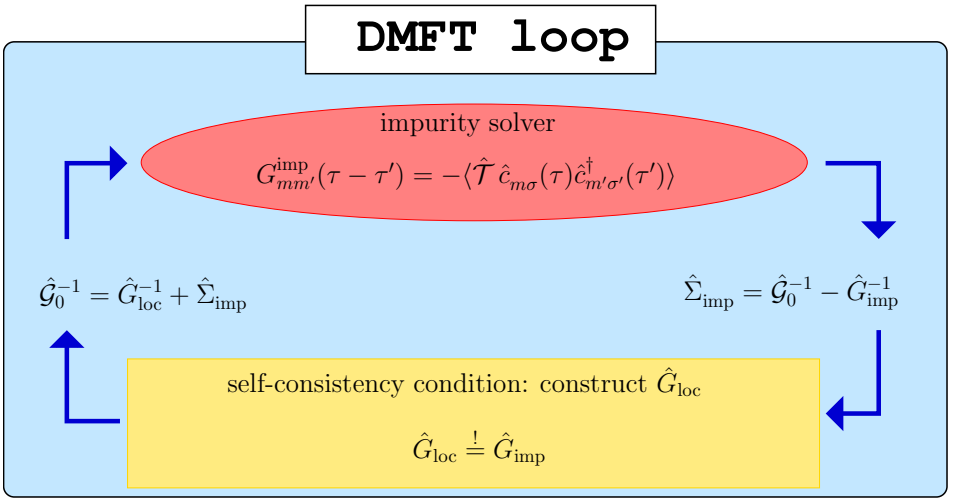

Fig. 1: *Self-consistency loop of DMFT. The heavy task is performed by the impurity solver, computing the impurity Green function, e.g., in imaginary time τ using quantum Monte Carlo.*

with $\beta = 1/T$ and where the matrix elements are reminiscent to their real-space analog (6). Note that both approaches display no true frequency dependence, the second factor in each expression, respectively, merely represents the simplest form of temperature dependence via the effect of the Fermi function. But importantly, frequency (or energy) dependence is a very relevant issue for describing interacting electrons: it regulates the impact of correlations on *different* energy scales due to the electrons' Janus-faced character hesitating between itinerancy and localization.

Eventually, DMFT is a theory that is designed to take care of that. Originally, it assumes a strong, i.e., only weakly-screened, *local* Coulomb interaction U effective on each lattice site. Then, in order to keep the full frequency dependence, but in the same time keeping the formalism operable, one drops the k dependence in the self-energy, i.e.

$$G^{\mathrm{DMFT}}(\mathbf{k}, i\omega_{\mathrm{n}}) := \big(i\omega_{\mathrm{n}} + \mu - H(\mathbf{k}) - \Sigma_{\mathrm{imp}}(i\omega_{\mathrm{n}})\big)^{-1}. \tag{23}$$

The self-energy $\Sigma_{\mathrm{imp}}(i\omega_{\mathrm{n}})$ is then linked to a quantum-impurity problem of the general form

$$\Sigma_{\mathrm{imp}}(i\omega_{\mathrm{n}}) = \mathcal{G}_0(i\omega_{\mathrm{n}})^{-1} - G_{\mathrm{imp}}(i\omega_{\mathrm{n}})^{-1}, \tag{24}$$

where the so-called *Weiss field* $\mathcal{G}_0(i\omega_{\mathrm{n}})$ is a unique function of the local Hamiltonian (expressed within a localized basis). To close the equations, the DMFT self-consistency condition reads

$$G^{\mathrm{DMFT}}_{\mathrm{loc}}(i\omega_{\mathrm{n}}) = \sum_{\mathbf{k}} [i\omega_{\mathrm{n}} + \mu - H(\mathbf{k}) - \Sigma_{\mathrm{imp}}(i\omega_{\mathrm{n}})]^{-1} \stackrel{!}{=} G_{\mathrm{imp}}(i\omega_{\mathrm{n}})\ . \tag{25}$$

The resulting iterative loop that is thereby implied to converge the DMFT self-energy is depicted in Fig. 1. Drawing a conceptual parallel between DFT and DMFT, while the former theory maps the interacting-electron problem onto the problem of non-interacting electrons in a highly-complicated potential, DMFT maps it to the problem of an interacting site within a self-consistent bath.

The challenging part is given by solving the quantum-impurity problem, to be done, e.g., with quantum Monte Carlo, Exact Diagonalization, etc.. Note that many-body wise, local-interaction diagrams are included to all orders in this non-perturbative theory. The vital energy dependence of the Weiss field ensures the qualitatively correct description of low-energy quasiparticle (QP) features as well as high-energy incoherent (Hubbard) excitations. Extensions to overcome the restriction to a k-independent self-energy, e.g., via cluster schemes, are available. But those will not be further pursued in the present text.
As for the previous approaches, charge self-consistency holds also for the DMFT method. But the issue of "self-consistency" has a more intriguing character than in Hartree-Fock and DFT. First, identical to these approaches, it serves to actually render the framework computationally feasible via the loop in Fig 1. But second, we deal with the structure of an explicit mean-field theory. This means that we replace the true surrounding of an interacting site by a *field*. This replacement itself is not an approximation, since "someone" could endow us with the exact field, just as "someone" could provide us the exact exchange-correlation functional in DFT. However here, we define this field by our self-consistent mean-field construction, hence marking the approximation.

2.4 Mixing

Before we move on to discuss the combined approach of DFT and DMFT in the next section, a few technical comments in view of solving the encountered self-consistency cycles are in order. In practice, the sketched flowcharts of iterating potentials (or self-energies) by directly replacing input- and output functions in a p-step process are in most cases extremely unstable. One needs to damp the whole iteration, usually via "mixing in" the potentials from previous steps, i.e.,

$$v^{(p+1)} = v^{(p+1)}(v^{(p)}, v^{(p-1)}, \ldots) \; . \tag{26}$$

Linear mixing is the simplest form of this and reads

$$v_{\mathrm{inp}}^{(p+1)} = (1-\alpha)\, v_{\mathrm{inp}}^{(p)} + \alpha\, v_{\mathrm{out}}^{(p)} \, , \qquad 0 < \alpha < 1 \; , \tag{27}$$

with $v_{\mathrm{inp(out)}}^{(p)}$ as the input(output) of step p. This means, not the straightforward output potential $v_{\mathrm{out}}^{(p)}$ is used for the input potential in step $p+1$, but a weighted mixture of the old input potential $v_{\mathrm{inp}}^{(p)}$ and $v_{\mathrm{out}}^{(p)}$. With a small enough mixing parameter α, convergence is nearly always ensured, yet then at the price of a slow and inefficient performance. More sophisticated variations of this kind of mixing, such as, e.g., *Anderson mixing*, may accelerate the convergence.
The mixing problem can also be approached more rigorously by formulating the search for a self-consistent solution as a root-finding problem of a tailored functional:

$$\mathcal{F}[v_{\mathrm{inp}}] = v_{\mathrm{out}}[v_{\mathrm{inp}}] - v_{\mathrm{inp}} \stackrel{!}{=} 0 \, . \tag{28}$$

As it is known from schooldays for ordinary functions $f(x)$, the Newton-Raphson method which involves the first derivative $f'(x)$ deals with such a task. Similarly, for our problem

the first derivative of $\mathcal{F}$ is needed which corresponds in physical terms to the dielectric function $\epsilon(\mathbf{r}, \mathbf{r}')$ or in mathematical terms to the Jacobian matrix $\mathbf{J}$. However, computing this first derivative may be cumbersome and often also the resulting mixing based on that generalized Newton-Raphson scheme turns out too hard. It proves more successful to invoke another scheme for an iterative approximation of the Jacobian matrix (or variations thereof). Those so-called *quasi-Newton schemes* with the *Broyden method* as its most familiar representative improve in every iteration step the approximation to $\mathbf{J}$ and are rather powerful in solving the mixing problem (28) especially for high-dimensional energy landscapes.
A good mixing scheme is very important to converge (or accelerate the convergence of) non-trivial self-consistency loops. In some cases, as, e.g., for many DMFT self-energies with statistical errors due to quantum Monte-Carlo, linear mixing may be sufficient. But especially for variational (saddle-point) problems, the mixing method often eventually decides if the whole framework converges and yields exploitable results. So even if "mixing" is not a highlighted physics theory like DFT or DMFT, it is very worthy and pays off to invest some time in dealing with it.

3 Realistic many-body account of correlated materials

Correlated materials are insufficiently described by DFT with conventional exchange-correlation functionals. There are static improvements, e.g., via methods like self-interaction correction, DFT+U, or hybrid functionals. While such schemes may mimic some physics of Mott-insulating systems, they usually show substantial deficiencies for the most-challenging problem of strongly correlated metals with a large deal of quantum fluctuations. The DMFT approach on the other hand is too heavy to be implemented in a complete realistic setting, since only a number of $M < 10$ local orbitals can so far be handled in accurate quantum-impurity solvers. Therefore, the hybrid approach of DFT and DMFT early on appeared as a natural combination to tackle electronic correlations on a realistic level beyond model-Hamiltonian descriptions. And indeed, nowadays the DFT+DMFT framework belongs to the hallmark electronic structure approaches, and is unrivaled within the field of strongly correlated materials.

3.1 Combining DFT and DMFT: functionals

Our introduction to DFT+DMFT starts on a formal level, to convince the reader that though this approach has a hybrid character, it is by no means a wild heuristic patchwork method leading to all kind of unphysical results. On the contrary, it is a physical and mathematically well-defined formalism built upon on a rock-solid functional description (for details see e.g. Refs. [7, 8]).
The idea is to identify a so-called *correlated subspace* $\mathcal{C}$ in a complete DFT-pictured electronic system, e.g., a $3d$ orbital manifold on a selected lattice site, where a DMFT treatment is necessary. First, we try to collect all relevant functions that govern such a combined scheme. From the DFT side, the electronic charge density ρ and the Kohn-Sham potential v_{KS} come to our mind. From the DMFT side in the correlated subspace, it is expected that the Green function

$G_\mathcal{C}$ as well as the self-energy $\Sigma_\mathcal{C}$ matter. The potential $v_{\rm KS}$ and the self-energy $\Sigma_\mathcal{C}$ serve as sources from a field-theoretical perspective. Note that ρ and $G_\mathcal{C}$ are independent, since there is no way to reconstruct the full real-space charge density from a given Green function in $\mathcal{C}$. By hand, we need to account for a double-counting (DC) correction, since electron-electron interaction in $\mathcal{C}$ is treated in both, DMFT *and* DFT, and enters the definition of $\Sigma_\mathcal{C}$.
The free energy of the whole system may than represented by the general *Baym-Kadanoff functional* form

$$\Omega[\mathbf{G}] = \mathrm{Tr}\ln\mathbf{G} - \mathrm{tr}\,\left((\mathbf{G}_0^{-1} - \mathbf{G}^{-1})\,\mathbf{G}\right) + \Phi[\mathbf{G}]\,, \tag{29}$$

with $\mathbf{G}$ as the full system Green function, $\mathbf{G}_0$ as the non-interacting Green function. The expression $\Phi[\mathbf{G}]$ marks the *Luttinger-Ward functional*, which describes the universal part of interacting electron systems. The Baym-Kadanoff representation of a DFT+DMFT system accordingly reads, avoiding explicit matrix notation,

$$\begin{aligned}\Omega_{\rm DFT+DMFT}[\rho, G_\mathcal{C}; v_{\rm KS}, \Sigma_\mathcal{C}] = &-\mathrm{Tr}\ln\Big(i\omega_n + \mu + \frac{1}{2m}\Delta - v_{\rm KS}(\mathbf{r}) - P^\dagger\Sigma_\mathcal{C}(i\omega_n)P\Big)\\ &- \int d\mathbf{r}\,\big(v_{\rm KS}(\mathbf{r}) - v_{\rm ext}(\mathbf{r})\big)\rho(\mathbf{r}) - \mathrm{Tr}\,\big(G_\mathcal{C}(i\omega_n)\Sigma_\mathcal{C}(i\omega_n)\big)\\ &+ E_{\rm H}[\rho(\mathbf{r})] + E_{\rm xc}[\rho(\mathbf{r})] + \Phi_\mathcal{C}[G_\mathcal{C}(i\omega_n)]\,.\end{aligned} \tag{30}$$

The objects $P, P^\dagger$ are projection operators that here "upfold" the self-energy $\Sigma_\mathcal{C}$ from the correlated subspace to the full Hilbert space of the system. The given functional can readily be varied with respect to our source terms, resulting in the known expressions for the charge density and the Green function $G_\mathcal{C}$

$$\frac{\delta\Omega}{\delta v_{\rm KS}} = 0 \qquad \Rightarrow \qquad \rho(\mathbf{r}) = \frac{1}{\beta}\sum_n \langle\mathbf{r}|\hat{G}|\mathbf{r}\rangle\,, \tag{31}$$

$$\frac{\delta\Omega}{\delta\Sigma_\mathcal{C}} = 0 \qquad \Rightarrow \qquad G_\mathcal{C}(i\omega_n) = P\,G(i\omega_n)\,P^\dagger\,, \tag{32}$$

with

$$\hat{G} = \Big(i\omega_n + \mu - \hat{H}_{\rm KS} - \hat{P}^\dagger\,\hat{\Sigma}_\mathcal{C}\,\hat{P}\Big)^{-1}. \tag{33}$$

Equations (31) and (32) are very important for several reasons: They make clear, that although ρ and $G_\mathcal{C}$ are independent, there is surely a coupling via the full Green function. Charge self-consistency is implied when converging the general charge density, carrying the effects from DFT as well as DMFT. Furthermore, the "downfolding" from the full Hilbert space to the correlated subspace again via the projection operators $P, P^\dagger$ is described. It becomes also obvious that our original set of governing functions is overcomplete, as at a stationary point the potential $v_{\rm KS}$ and the self-energy $\Sigma_\mathcal{C}$ are direct functions of ρ and $G_\mathcal{C}$. To explore this, one may formally write $\tilde{\Omega}_{\rm DFT+DMFT}[\rho, G_\mathcal{C}; v_{\rm KS}, \Sigma_\mathcal{C}] = \Omega_{\rm DFT+DMFT}[\rho, G_\mathcal{C}; v_{\rm KS}[\rho, G_\mathcal{C}], \Sigma_\mathcal{C}[\rho, G_\mathcal{C}]]$ and perform

$$\frac{\delta\tilde{\Omega}}{\delta\rho} = 0 \qquad \Rightarrow \qquad v_{\rm KS}(\mathbf{r}) = v_{\rm ext}(\mathbf{r}) + v_{\rm H}(\mathbf{r}) + v_{\rm xc}(\mathbf{r})\,, \tag{34}$$

$$\frac{\delta\tilde{\Omega}}{\delta G_\mathcal{C}} = 0 \qquad \Rightarrow \qquad \Sigma_\mathcal{C}(i\omega_n) = \frac{\delta\Phi_\mathcal{C}}{\delta G_\mathcal{C}} := \Sigma_{\rm imp}(i\omega_n) - \Sigma_{\rm DC}\,, \tag{35}$$

whereby we introduced the DC correction Σ_{DC}. Thus formally, the original relations for the Kohn-Sham potential and the DMFT self-energy are retained. The set of equations (31-35) define the working scheme of the DFT+DMFT approach.
Let us finally find an expression for the total energy. By defining the Kohn-Sham Green function

$$G_{\mathrm{KS}}(\mathbf{k}, i\omega_n) := \left(i\omega_n + \mu - \varepsilon^{\mathrm{KS}}_{\mathbf{k}}\right)^{-1} \tag{36}$$

one can rewrite the free-energy functional as

$$\Omega_{\mathrm{DFT+DMFT}} = \Omega_{\mathrm{DFT}} + \mathrm{Tr}\ln G^{-1}_{\mathrm{KS}} - \mathrm{Tr}\ln G^{-1} - \mathrm{Tr}(G_{\mathcal{C}}\Sigma_{\mathcal{C}}) + \Phi_{\mathcal{C}}\ , \tag{37}$$

where Ω_{DFT} is the free-energy analog to expression (14). For $T \to 0$, this leads to

$$E_{\mathrm{DFT+DMFT}} = E_{\mathrm{DFT}} - \sum_{\mathbf{k}\nu} \varepsilon^{\mathrm{KS}}_{\mathbf{k}\nu} + \mathrm{Tr}(GH_{\mathrm{KS}}) + \mathrm{Tr}(G_{\mathcal{C}}\Sigma_{\mathrm{imp}}) - E_{\mathrm{DC}}\ . \tag{38}$$

In this total-energy formula, the term E_{DFT} corresponds to (18) and $\varepsilon^{\mathrm{KS}}_{\mathbf{k}\nu}$ are the Kohn-Sham eigenvalues with band index ν and E_{DC} is the double-counting correction to the energy. Note that the band sum $\sum_{\mathbf{k}\nu} \varepsilon^{\mathrm{KS}}_{\mathbf{k}\nu} = \mathrm{Tr}(G_{\mathrm{KS}}H_{\mathrm{KS}})$ is already included in E_{DFT} and has to be subtracted, as it is replaced by the interaction-dressed $\mathrm{Tr}(GH_{\mathrm{KS}})$. Importantly, in the latter term the trace is performed with respect to the full interacting Green function G.
This concludes the formal discussion of the DFT+DMFT scheme and we will turn in the next section to the more practical aspects of an implementation of it.

3.2 Combining DFT and DMFT: in practice

First concrete implementations of the DFT+DMFT approach appeared at the end of the 1990s [9, 10]. Those original schemes performed in a so-called "one-shot" or "post-processing" manner. After a converged DFT calculation, the density of states (and later the full Kohn-Sham Hamiltonian H_{KS}) of the correlated subspace $\mathcal{C}$ entered an otherwise disjunct DMFT calculation. Hence within the one-shot approach, there was no feedback of the DMFT self-energy on the general electronic structure and charge self-consistency is not reached.
State-of-the-art implementations of the full scheme are charge self-consistent (e.g. [11–14]). A pictorial sketch of the framework, in line with the demonstrations in the last subsection, is given in Fig. 2. Both original self-consistency cycles of DFT and DMFT are interweaved to establish a novel self-consistent solution for the realistic correlated electronic structure. It becomes obvious, that especially the link between both traditional schemes, i.e., the down- and upfolding to/from the correlated subspace, is key to the method. As $\mathcal{C}$ is by definition a local region in real space, a (partly) local-orbital representation is thus an essential building block of the DFT+DMFT framework [15]. Linear-muffin-tin-orbitals [16], Wannier(like) functions, e.g., of maximally-localized kind [17], or projected-local orbitals [18, 19] may provide a convenient representation thereof.
In the following, the implementation based on projected-local orbitals will be discussed (see Ref. [18] for more details). Let us start by defining $m = 1, \ldots, M$ orthonormal orbitals $\{\chi^{\mathbf{R}}_m\}$ on the

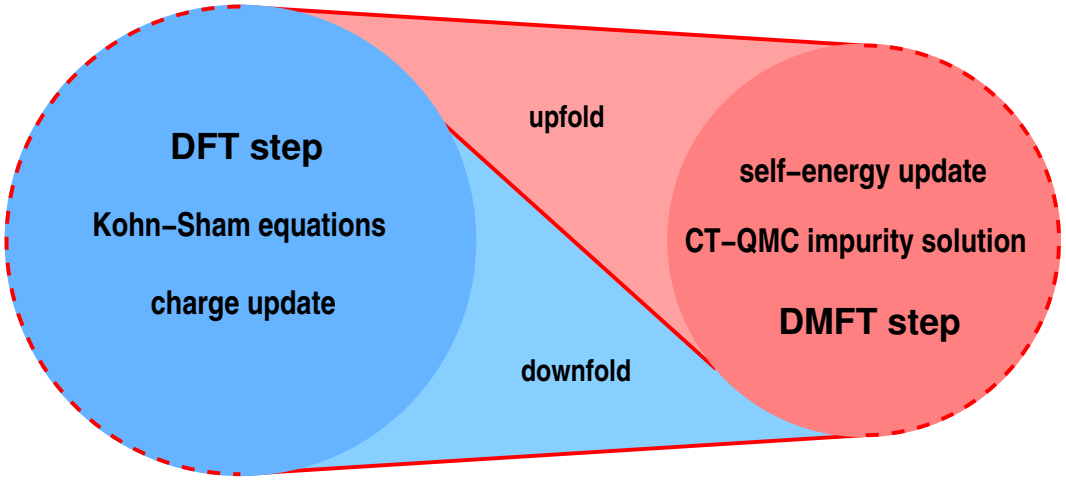

Fig. 2: *State-of-the-art charge self-consistent DFT+DMFT loop. The calculation usually starts from a self-consistent Kohn-Sham solution. The correlated subspace is defined and the initial Weiss field $\mathcal{G}_0$ constructed. Afterwards, a single (or more) DMFT step(s) is(are) performed. The impurity solution may, e.g., be achieved with the continuous-time quantum Monte-Carlo (CT-QMC) method. The obtained self-energies are upfolded and an updated charge density $\rho(\mathbf{r})$ is computed. A new charge density implies a new Kohn-Sham potential, and a single new Kohn-Sham step is performed, from which a new Weiss field is generated, etc..*

lattice site $\mathbf{R}$ in $\mathcal{C}$. By the use of the complete set of KS states $\{\psi_{\mathbf{k}\nu}\}$ at point k in reciprocal space, the Bloch transform of these local orbitals may be expressed via

$$|\chi^{\mathbf{R}}_{\mathbf{k}m}\rangle := \sum_{\mathbf{T}} \mathrm{e}^{i\mathbf{k}\cdot(\mathbf{T}+\mathbf{R})}|\chi^{\mathbf{R}}_{m}\rangle = \sum_{\nu} |\psi_{\mathbf{k}\nu}\rangle\langle\psi_{\mathbf{k}\nu}|\chi^{\mathbf{R}}_{\mathbf{k}m}\rangle = \sum_{\nu}\langle\psi_{\mathbf{k}\nu}|\chi^{\mathbf{R}}_{\mathbf{k}m}\rangle\,|\psi_{\mathbf{k}\nu}\rangle\ , \tag{39}$$

whereby $\mathbf{T}$ denotes a Bravais lattice vector and the sum over ν covers the whole set of bands. Thus the Bloch transform represents a *Wannier function*. To render the approach more flexible, it proves useful to extend the concept of the correlated subspace also to energy space and to permit a restriction in the noted band sum to an energy window $\mathcal{W}$, i.e.

$$|\tilde{\chi}^{\mathbf{R}}_{\mathbf{k}m}\rangle = \sum_{\nu\in\mathcal{W}}\langle\psi_{\mathbf{k}\nu}|\chi^{\mathbf{R}}_{\mathbf{k}m}\rangle\,|\psi_{\mathbf{k}\nu}\rangle\ . \tag{40}$$

The resulting Bloch transform is then not anymore a true Wannier function. Yet one may promote it to one by proper orthonormalization

$$|w^{\mathbf{R}}_{\mathbf{k}m}\rangle = \sum_{\mathbf{R}'m'}\left(O(\mathbf{k})^{-1/2}\right)^{\mathbf{R}\mathbf{R}'}_{mm'}|\tilde{\chi}^{\mathbf{R}'}_{\mathbf{k}m'}\rangle\ , \tag{41}$$

using the overlap matrix $O^{\mathbf{R}\mathbf{R}'}_{mm'}(\mathbf{k}) := \langle\tilde{\chi}^{\mathbf{R}}_{\mathbf{k}m}|\tilde{\chi}^{\mathbf{R}'}_{\mathbf{k}m'}\rangle$. To enable flexible transformations between the system's complete Bloch space (spanned by $\{\psi_{\mathbf{k}\nu}\}$) and the correlated subspace (spanned by $\{w^{\mathbf{R}}_{\mathbf{k}m}\}$) it proves useful to define the projection functions

$$P^{\mathbf{R}}_{m\nu}(\mathbf{k}) := \sum_{\mathbf{R}'m'}\left(O(\mathbf{k})^{-1/2}\right)^{\mathbf{R}\mathbf{R}'}_{mm'}\langle\chi^{\mathbf{R}}_{\mathbf{k}m}|\psi_{\mathbf{k}\nu}\rangle\ . \tag{42}$$

For instance, the transformation from Bloch to Wannier space readily reads

$$|w^{\mathbf{R}}_{\mathbf{k}m}\rangle = \sum_{\nu \in \mathcal{W}} P^{\mathbf{R}*}_{\nu m}(\mathbf{k})\, |\psi_{\mathbf{k}\nu}\rangle \ . \tag{43}$$

Assuming the full Green function operator of the system in the form (33), the Bloch Green function is given by

$$G^{\mathrm{Bloch}}_{\nu\nu'}(\mathbf{k}, i\omega_n) = \langle \psi_{\mathbf{k}\nu} | \hat{G} | \psi_{\mathbf{k}\nu'} \rangle \ . \tag{44}$$

The downfolding equation from Bloch space to correlated subspace for the Green function and the upfolding equation from $\mathcal{C}$ to Bloch space for the self-energy are then straightforwardly written as

$$G^{\mathbf{R}}_{mm'}(i\omega_{\mathrm{n}}) = \sum_{\mathbf{k},(\nu\nu')\in\mathcal{W}} P^{\mathbf{R}}_{m\nu}(\mathbf{k})\, G^{\mathrm{Bloch}}_{\nu\nu'}(\mathbf{k}, i\omega_{\mathrm{n}})\, P^{\mathbf{R}*}_{\nu' m'}(\mathbf{k}) \ , \tag{45}$$

$$\Sigma^{\mathrm{Bloch}}_{\nu\nu'}(\mathbf{k}, i\omega_{\mathrm{n}}) = \sum_{\mathbf{R},mm'} P^{\mathbf{R}*}_{\nu m}(\mathbf{k})\, \Sigma^{\mathbf{R}}_{mm'}(i\omega_{\mathrm{n}})\, P^{\mathbf{R}}_{m'\nu'}(\mathbf{k}) \ . \tag{46}$$

The local self-energy is given by the DMFT impurity solution corrected by the double-counting term through

$$\mathbf{\Sigma}^{\mathbf{R}}(i\omega_{\mathrm{n}}) = \mathbf{\Sigma}^{\mathbf{R}}_{\mathrm{imp}}(i\omega_{\mathrm{n}}) - \mathbf{\Sigma}^{\mathbf{R}}_{\mathrm{DC}} \ . \tag{47}$$

Once the upfolding of the self-energy to the whole space is achieved, the complete charge density $\rho(\mathbf{r})$ may be updated. At this point, a practical comment on the charge treatment in the different stages of the self-consistency cycle is in order. In principle, the sum rule for the total charge holds for the full DFT+DMFT charge density and the associated chemical potential μ. However, it is surely advisable to have the correct total charge of the system already within the DFT part of the calculation. Otherwise the numerics may be cumbersome due to an ill-defined Coulomb balance between electrons and nuclei. Therefore we redefine the Kohn-Sham Green function (36) as

$$G_{\mathrm{KS}}(\mathbf{k}, i\omega_n) := \left(i\omega_n + \mu_{\mathrm{KS}} - \varepsilon^{\mathrm{KS}}_{\mathbf{k}}\right)^{-1} , \tag{48}$$

with the chemical potential μ_{KS} chosen such as to enforce the correct total electronic charge $N = \int d\mathbf{r}\, \rho(\mathbf{r})$ in the DFT part. The full charge density is then split into two parts, namely

$$\rho(\mathbf{r}) = \rho_{\mathrm{KS}}(\mathbf{r}) + \Delta\rho(\mathbf{r}) = \frac{1}{\beta}\sum_n \Big(\langle \mathbf{r}|\hat{G}_{\mathrm{KS}}|\mathbf{r}\rangle + \langle \mathbf{r}|\hat{G} - \hat{G}_{\mathrm{KS}}|\mathbf{r}\rangle \Big) , \tag{49}$$

with $\hat{G}_{\mathrm{KS}}$ in analogy to (36). Since due to our choice of ρ_{KS} already carrying the total charge, the correction term $\Delta\rho$ amounts to a redistribution of the charge density such that $\int d\mathbf{r}\, \Delta\rho(\mathbf{r}) = 0$ holds. The correction kernel beyond DFT can also be rewritten as

$$\langle \mathbf{r}|\hat{G} - \hat{G}_{\mathrm{KS}}|\mathbf{r}\rangle = \langle \mathbf{r}|\hat{G}_{\mathrm{KS}}(\hat{G}^{-1}_{\mathrm{KS}} - \hat{G}^{-1})\hat{G}|\mathbf{r}\rangle = \langle \mathbf{r}|\hat{G}_{\mathrm{KS}}\left(\hat{\Sigma}^{\mathrm{Bloch}} - (\mu - \mu_{\mathrm{KS}})\hat{1}\right)\hat{G}|\mathbf{r}\rangle \ . \tag{50}$$

If we then define

$$\Delta N_{\nu\nu'}(\mathbf{k}) := \frac{1}{\beta}\sum_{n,\nu''\nu'''\in\mathcal{W}} G^{\mathrm{KS}}_{\nu\nu''}(\mathbf{k}, i\omega_{\mathrm{n}}) \Big(\Sigma^{\mathrm{Bloch}}_{\nu''\nu'''}(\mathbf{k}, i\omega_{\mathrm{n}}) - (\mu - \mu_{\mathrm{KS}})\, \delta_{\nu''\nu'''} \Big) G_{\nu'''\nu'}(\mathbf{k}, i\omega_{\mathrm{n}}), \tag{51}$$

the charge-correction term $\Delta\rho$ reads

$$\Delta\rho(\mathbf{r}) = \sum_{\mathbf{k},\nu\nu'\in\mathcal{W}} \langle\mathbf{r}|\psi_{\mathbf{k}\nu}\rangle\, \Delta N_{\nu\nu'}(\mathbf{k})\, \langle\psi_{\mathbf{k}\nu'}|\mathbf{r}\rangle\,. \tag{52}$$

As the DFT contribution ρ_{KS} is by definition diagonal in the band indices, the complete correlated charge density after a DFT+DMFT step reads

$$\rho(\mathbf{r}) = \sum_{\mathbf{k},\nu\nu'} \langle\mathbf{r}|\psi_{\mathbf{k}\nu}\rangle \Big(f(\tilde{\varepsilon}^{\mathrm{KS}}_{\mathbf{k}\nu})\, \delta_{\nu\nu'} + \Delta N_{\nu\nu'}(\mathbf{k}) \Big) \langle\psi_{\mathbf{k}\nu'}|\mathbf{r}\rangle\ , \tag{53}$$

where f is the Fermi-Dirac function and $\tilde{\varepsilon}^{\mathrm{KS}}_{\mathbf{k}\nu} = \varepsilon^{\mathrm{KS}}_{\mathbf{k}\nu} - \mu_{\mathrm{KS}}$. Thus, because of the inadequacy of a pure band picture of strongly correlated materials additional off-diagonal terms in the band index contribute in the many-body system with additional real-space excitations. This updated charge density then defines a new Kohn-Sham effective potential v_{KS} and the charge self-consistency loop is closed.

Let us at the end of this section briefly comment on additional aspects of the DFT+DMFT formalism. So far, we did not say anything at all about the interacting Hamiltonian that governs the correlated subspace and which explicitly enters the DMFT iterations. Basically, one utilizes an m-orbital generalized Hubbard Hamiltonian, e.g., of Slater-Kanamori type

$$\begin{aligned}
\hat{H}^{\mathcal{C}}_{\mathrm{int}} = & \sum_{\langle\mathbf{R}\mathbf{R}'\rangle mm'\sigma} t^{mm'}_{\mathbf{R}\mathbf{R}'}\, \hat{c}^{\dagger}_{\mathbf{R}m\sigma}\hat{c}_{\mathbf{R}'m'\sigma} + U \sum_{i\mathbf{R}m} \hat{n}_{\mathbf{R}m\uparrow}\hat{n}_{\mathbf{R}m\downarrow} \\
& + \frac{1}{2} \sum_{\mathbf{R},m\neq m',\sigma} \Big((U-2J_{\mathrm{H}})\, \hat{n}_{\mathbf{R}m\sigma}\hat{n}_{\mathbf{R}m'\bar{\sigma}} + (U-3J_{\mathrm{H}})\, \hat{n}_{\mathbf{R}m\sigma}\hat{n}_{\mathbf{R}m'\sigma} \Big) \\
& + \frac{1}{2} \sum_{\mathbf{R}m\neq m',\sigma} J_{\mathrm{H}} \left(\hat{c}^{\dagger}_{\mathbf{R}m\sigma}\hat{c}^{\dagger}_{\mathbf{R}m'\bar{\sigma}}\hat{c}_{\mathbf{R}m\bar{\sigma}}\hat{c}_{\mathbf{R}m'\sigma} + \hat{c}^{\dagger}_{\mathbf{R}m\sigma}\hat{c}^{\dagger}_{\mathbf{R}m\bar{\sigma}}\hat{c}_{\mathbf{R}m'\bar{\sigma}}\hat{c}_{\mathbf{R}m'\sigma} \right).
\end{aligned} \tag{54}$$

Here, $\boldsymbol{t}$ refers to the Kohn-Sham hopping matrix, U marks the Hubbard interaction, J_{H} the Hund's exchange and $\hat{n} = \hat{c}^{\dagger}\hat{c}$. For a discussion of this and related Hamiltonians we refer to [20]. The DMFT impurity solution subject to such Hamiltonian forms may nowadays, e.g., be obtained from the continuous-time quantum Monte-Carlo (CT-QMC) method (see e.g. Ref. [21] for a review). The interaction parameters are either chosen from a reasonable guess (often by connecting also to experimental data) or are computed from first-principles schemes such as the constrained random-phase approximation (cRPA).

The issue of double-counting is a well-known feature of DFT+DMFT and various forms are available for the correction term Σ_{DC}. Since conventional DFT exchange-correlation functionals are not representable within standard many-body diagrams, a straightforward analytical solution of the DC problem is not available. Usually, the double counting is assumed orbital independent (i.e. spherical) and a commonly used formula is based on the so-called fully-localized or atomic limit [22]

$$\Sigma^{\mathrm{DC}}_{\mathbf{R}m\sigma} = U \left((\langle\hat{n}_{\mathbf{R}}\rangle - \frac{1}{2} \right) - J_{\mathrm{H}} \left(\langle\hat{n}_{\mathbf{R}\sigma}\rangle - \frac{1}{2} \right). \tag{55}$$

Albeit the general topic is heavily debated, nonetheless, many results on the qualitative and even (semi)-quantitative physics of strongly correlated materials are not that sensitive to the details of double counting. Otherwise the DFT+DMFT approach would not be that successful. A solution to the DC problem may be achieved by abandoning the concrete KS-DFT environment and replace it by a true (weakly-correlated) many-body setting. The numerically very heavy GW+DMFT scheme [23] provides such a description.
Finally, note that in various multi-atom unit cells, the correlated subspace is often not only associated with a single lattice site, as already anticipated in our sums over the sites $\mathbf{R}$ (e.g. in eq. (46)). For symmetry-equivalent sites, it suffices to compute the self-energy for a representative site and transfer it to the remaining sites via proper symmetry relations. In the case of various sites which are inequivalent by symmetry, e.g., the Fe sites with octahedral or tetrahedral environment in magnetite Fe_3O_4, a different impurity problem is defined for each symmetry-inequivalent site $\mathbf{R}$ through [24]

$$\mathcal{G}_0^{\mathbf{R}}(i\omega_{\mathrm{n}})^{-1} = G^{\mathbf{R}}(i\omega_{\mathrm{n}})^{-1} + \Sigma_{\mathrm{imp}}^{\mathbf{R}}(i\omega_{\mathrm{n}}), \tag{56}$$

and the coupling is realized via the DFT+DMFT self-consistency condition invoking the computation of the complete lattice Green function.

3.3 Relevance of charge self-consistency

There is surely an intuitive believe that charge self-consistency is a good thing to have in an electronic structure calculation. But let us try to identify concrete features from a DFT+DMFT perspective that renders it superior to the simpler one-shot framework. Before doing so, one should mention that charge self-consistent DFT+DMFT calculations are numerically heavier than the latter. Not only because of the additional solution of a DFT problem at each iteration step, though especially for large supercell computations this further effort is still not negligible. What matters more is the usually slower convergence when demanding charge self-consistency, since the correlation-induced charge redistributions need additional numerical steps to settle.
Concerning the advantageous features, several points are noteworthy. First, the orbital occupations within the correlated subspace are due to change because of the relaxing surrounding electron structure. Second, importantly, the remaining electronic structure *outside* the correlated subspace $\mathcal{C}$ (i.e. ligand states, etc.) may also "react" to the local-Coulomb effect within $\mathcal{C}$. The interweaving of both of these effects is very important for, e.g., orbital polarizations, local magnetic moments, magnetic exchange, and, not to forget, the total energy $E_{\mathrm{DFT+DMFT}}$. Thus, for instance, even if the local orbital occupations within $\mathcal{C}$ do not change much with charge self-consistency, the effect on a possible magnetic ordering may still be crucial.
It is obvious that the degree of correlation-induced charge redistributions also depends on the symmetry of the system. In highly-symmetric compounds, such as the cubic perovskite and "DMFT pet" $SrVO_3$, the impact of charge self-consistency is expected to be minor. But for lower-symmetry problems, often associated with various symmetry-inequivalent sites (such as oxide heterostructures), the effects can be crucial. Furthermore, for materials close to a Mott

transition, the systems are very susceptible to perturbations in the electronic structure, and charge self-consistency can have obvious qualitative effects, even if the crystal symmetry is seemingly high. We will discuss in section 4 the metal-insulator transition in V_2O_3 as a prominent example.
Two general features are often observed in charge self-consistent DFT+DMFT. In cases where one-shot calculations lead to strong orbital polarization, e.g., within a crystal-field split $3d(t_{2g})$ manifold, charge self-consistency weakens this tendency. This is understandable from the fact that a strong orbital polarization affects the ligand neighborhood in order to relax the electronic structure. This relevant "reaction" of the neighboring electrons has usually the effect of screening the original strong orbital polarization, i.e., reducing it from its one-shot magnitude. Second, it is furthermore observed that charge self-consistency tends to wash out differences between varying double-counting schemes [25].

4 An illustrative materials example: Metal-insulator transition in V_2O_3

After all the formal theory, the last section shall be used to discuss a concrete application of charge self-consistent DFT+DMFT to a challenging materials problem. We will realize that the theoretical description of the famous V_2O_3 problem, benefits strongly from charge self-consistency.

4.1 Phase diagram and basic materials characteristics

Since about fifty years, vanadium sesquioxide V_2O_3 poses a demanding problem in the understanding of correlated materials [26–28]. In the field of realistic interacting solid-state systems, the compound has without doubt the second most prominent phase diagram [26, 27], after the one of high-T_c cuprates. Its canonical finite-temperature form (see Fig. 3a) includes three key phases, namely a paramagnetic-metallic (PM) one, a paramagnetic-insulating (PI) one, and an antiferromagnetic-insulating (AFI) phase at finite T. At ambient T and pressure, the stoichiometric compound is stable in the PM phase with a corundum crystal structure, i.e., the system is metallic at room temperature. The corundum structure (cf. Fig. 3b) has trigonal symmetry with V dimers along the c-axis and a V-based honeycomb lattice in the ab-plane. Upon lowering the temperature, a metal-insulator transition (MIT) towards the AFI phase, with notably a monoclinic crystal structure, occurs at $T_N \sim 155$ K.
Formally, in V_2O_3, vanadium is in the oxidation state 3+, i.e., a valence configuration $3d^2$. Within the VO_6 octahedra, the V$(3d)$ manifold is first split into higher-energy e_g and lower-energy t_{2g} states due to the octahedral crystal field. Because of the tilted orientation of those octahedra, the additional trigonal crystal field splits threefold V-t_{2g} into a_{1g} and two degenerate e_g^π states. There are numerous DFT investigations of this compound [29–33]. On the corresponding level, a low-energy V-t_{2g} bandwidth of $W \sim 2.6$ eV (see Fig. 4), harboring the two electrons in the occupied part, results around the Fermi level ε_F. The a_{1g} orbital points along the

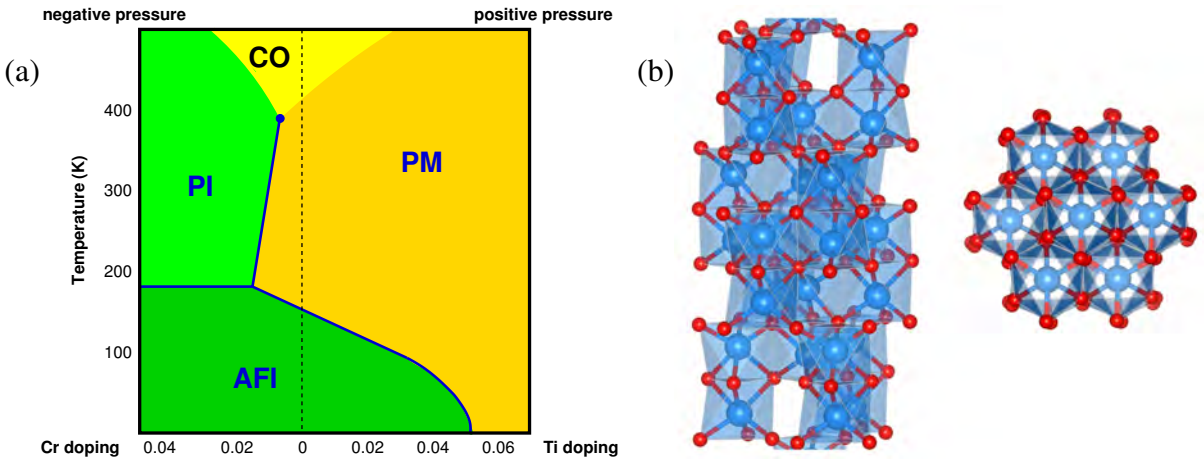

Fig. 3: *Basic information on V_2O_3. (a) Temperature vs. pressure/doping phase diagram with the following phases: paramagnetic metal (PM), paramagnetic insulator (PI) and antiferromagnetic insulator (AFI). The 'CO' area marks the PI-PM crossover region. (b) Corundum structure with V (blue) and O (red), left: view with c-axis vertical; and right: view along c-axis.*

c-axis and along the V-V dimers, which therefore display a pronounced bonding/anti-bonding splitting. The e_g^π orbitals point inbetween the oxygens and are expected to describe more localized behavior than a_{1g}. An orbital polarization $n(e_g^\pi)/n(a_{1g}) = 1.44/0.56 = 2.57$ in favor of e_g^π is obtained in DFT. Note that in the low-T monoclinic AFI phase, the V-V dimer distance *grows* and does not shrink as in the akin VO_2 compound. Thus a straightforward Peierls-like mechanism due to dimerization is not at the origin of the metal-insulator transition. But the in-plane degeneracy in the V-V distances within the honeycomb lattice is broken in the monoclinic phase. Thus after cubic and trigonal components in the crystal field, there is yet a further monoclinic one appearing, eventually splitting the e_g^π degeneracy. As seen in Fig. 3a, doping with Cr (or application of negative pressure) at ambient temperature results in another metal-insulator transition from the PM to the PI phase for about 1.5% of Cr dopants. This MIT is particularly interesting, since apparently no global symmetry is broken, i.e., the corundum symmetry and paramagnetism remain vital. Hence, seemingly, the V_2O_3 phase diagram displays all characteristics of a "model phase diagram" for a strongly correlated system on a lattice: strong electronic correlations create local magnetic moments that order at low temperature via a MIT in an antiferromagnetic phase; upon application of negative pressure the lattice expands and a different MIT occurs due to a reduction of the hopping, while application of positive pressure or Ti doping stabilizes the metal due to a strengthening of the hopping. So far, so nice. But this simplistic model picture of V_2O_3 has attained serious cracks over the many years of investigation, suggesting that especially the doping with Cr or Ti results in much more intriguing physics than originally envisioned. This lecture is not the place to go into full detail of this, but let us remark on only one relevant aspect (for more on this matter see, e.g., Ref. [34]). Though Cr(Ti) doping has the same phenomenological effect as negative(positive) pressure, i.e., driving localization(itinerancy), they do not coincide in terms of the microscopic mechanism. Namely, while Cr doping indeed expands the lattice [35], Ti doping does not contract the lattice, but actually also expands it (albeit not as strongly as Cr doping) [36].

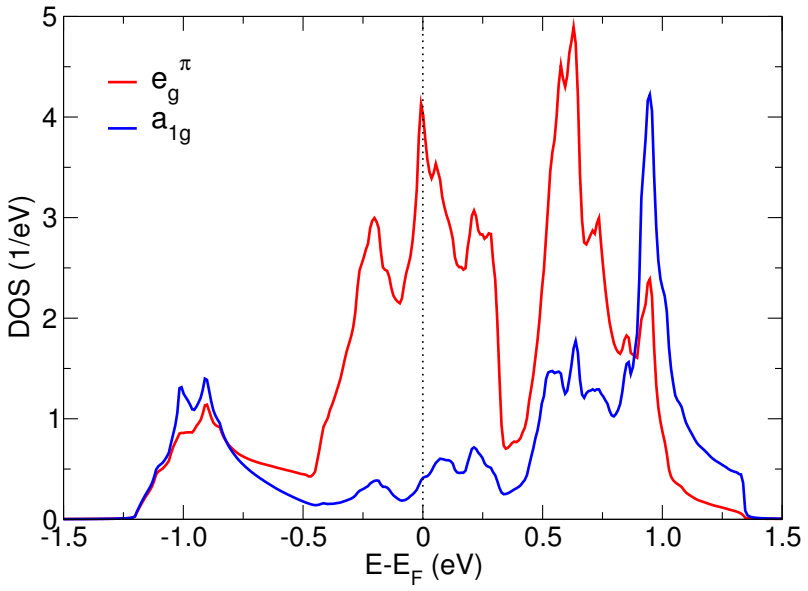

Fig. 4: *Local V-t_{2g} density of states (DOS) for V_2O_3.*

4.2 Electronic correlations within DFT+DMFT

When going beyond DFT for this strongly correlated material, the transition-metal t_{2g} electrons are usually chosen to form the correlated subspace of V_2O_3. An interacting Hamiltonian of Slater-Kanamori form (54), is conveniently governing this subspace. From a Hubbard $U\sim$5 eV, the ratio $U/W \sim 2$ puts the V_2O_3 system well into the strongly correlated regime. As the corundum structure builds up on two formula units in its primitive cell, there are four symmetry-equivalent V ions to take care of in multi-site DFT+DMFT. Also on the latter level, there exist already many studies for this hallmark material [37–39, 14, 40–43].

In the following, we want to the restrict the discussion to the paramagnetic regime. We set the local Coulomb interactions to $U = 5$ eV and $J_{\rm H} = 0.7$ eV and perform the calculations for $T = 387$ K ($\beta = 30$ eV^{-1}) and $T = 193$ K ($\beta = 60$ eV^{-1}). The focus is on two structural cases, namely the stoichiometric corundum unit-cell and the effective 2.8% Cr-doped corundum unit-cell, both based on the crystal data of Dernier [35]. Note importantly, that the cell with effective Cr doping differs only via the lattice parameters and the Wyckoff positions of V and O compared to the stoichiometric cell. In other words, the effect of 2.8% Cr dopants is taken into account only on the average by an effective refinement of the vanadium and oxygen positions. The explicit effects of the different valence of Cr compared to V as well as *local* structural relaxations due to Cr impurities are neglected. This approximation of the effect of Cr doping renders the computations in the doped case simple, but it is also a rough one. Nonetheless, this approximate treatment of Cr doping has nearly exclusively been used in former theoretical assessments of Cr-doped V_2O_3.

Figure 5 displays the k-integrated spectral functions $A(\omega)$ at stoichiometry and with effective Cr doping. From the total spectral functions, three observations are readily made. First, vanadium sesquioxide is indeed a strongly correlated material, since it shows a substantially renormalized quasiparticle peak and lower/upper Hubbard bands due to the spectral-weight

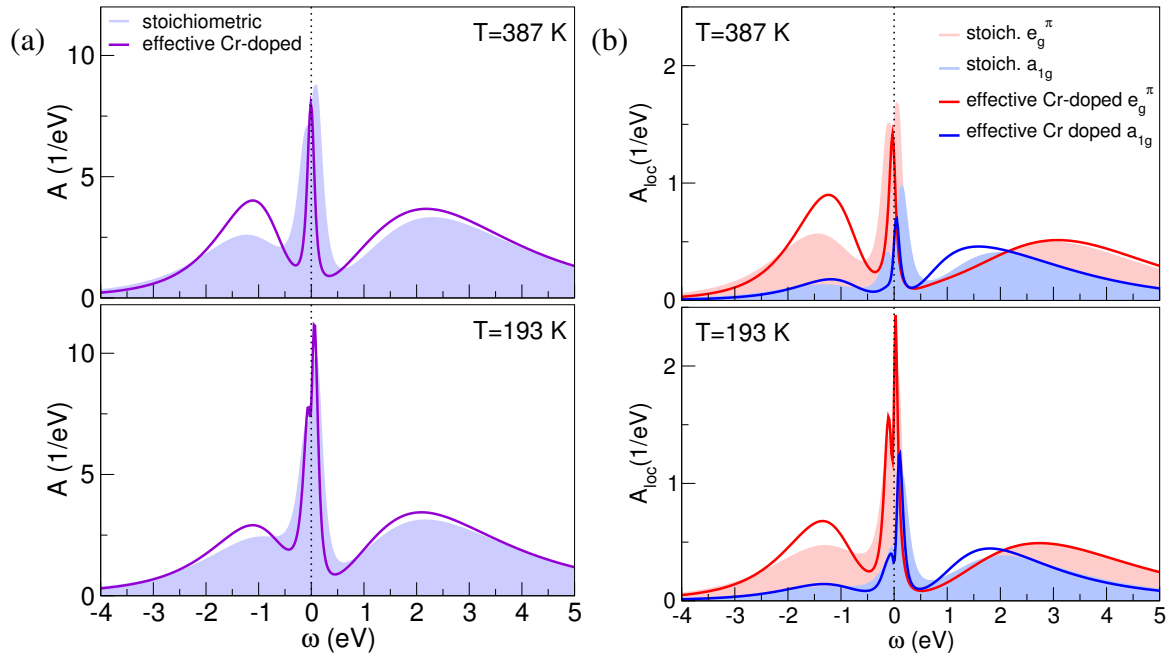

Fig. 5: *DFT+DMFT k-integrated spectral functions $A(\omega)$ for stoichiometric and effective Cr-doped (see text) V_2O_3 at $T = 387\,K$ (top) and $T = 193\,K$ (bottom), respectively. (a) total $A(\omega)$ and (b) local V-t_{2g} $A(\omega)$.*

transfer to incoherent local excitations at higher energy. Second, in line with the experimental phase diagram, with effective Cr doping the system is indeed more strongly correlated than at stoichiometry. Third, the spectral-weight transfer from low energy to high energy is stronger at *higher* temperatures. This means, that there is a rather small coherence scale of the QPs, leading to an increasing effective localization of the corresponding electrons for T larger than that scale. On the local level, the orbital polarization between e_g^π and a_{1g} is increased with correlations, actually from the DFT value $n(e_g^\pi)/n(a_{1g}) = 1.44/0.56$ to the DFT+DMFT values $n(e_g^\pi)/n(a_{1g}) = 1.58/0.42$ at stoichiometry and $n(e_g^\pi)/n(a_{1g}) = 1.60/0.40$ for effective Cr doping. The increase of orbital polarization is explained by a trigonal-crystal-field enhancement due to electronic correlations [38, 39].

For completeness, Fig. 6 exhibits the k-resolved spectral function of stoichiometric V_2O_3 along high-symmetry lines in the first Brillouin zone. Note that because of the strong correlations, the dispersion of the QPs is now "squeezed" in an energy window $[-0.3, 0.3]$ eV, whereas on the DFT level we remember an effective bandwidth of $W \sim 2.6$ eV. The spectral weight in this low-energy region is already substantially broadened, only along k_z, i.e., the line Z-Γ, displays a rather coherent QP part. The spectrum is in good agreement with recent angle-resolved photoemission (ARPES) experiments by Vecchio *et al.* [44], though the electron pocket at Γ is even deeper in energy within the experimental data.

Let us finally compare the electronic charge density $\rho(\mathbf{r})$ from DFT and from charge self-consistent DFT+DMFT. Figure 7a shows the bonding charge density $\rho_{\mathrm{bond}} = \rho - \rho_{\mathrm{atomic}}$ within the ab-plane of V_2O_3. The function ρ_{bond} is often more instructive than the pure ρ, since the latter is a large-valued function that mainly marks the ionic positions on the lattice with

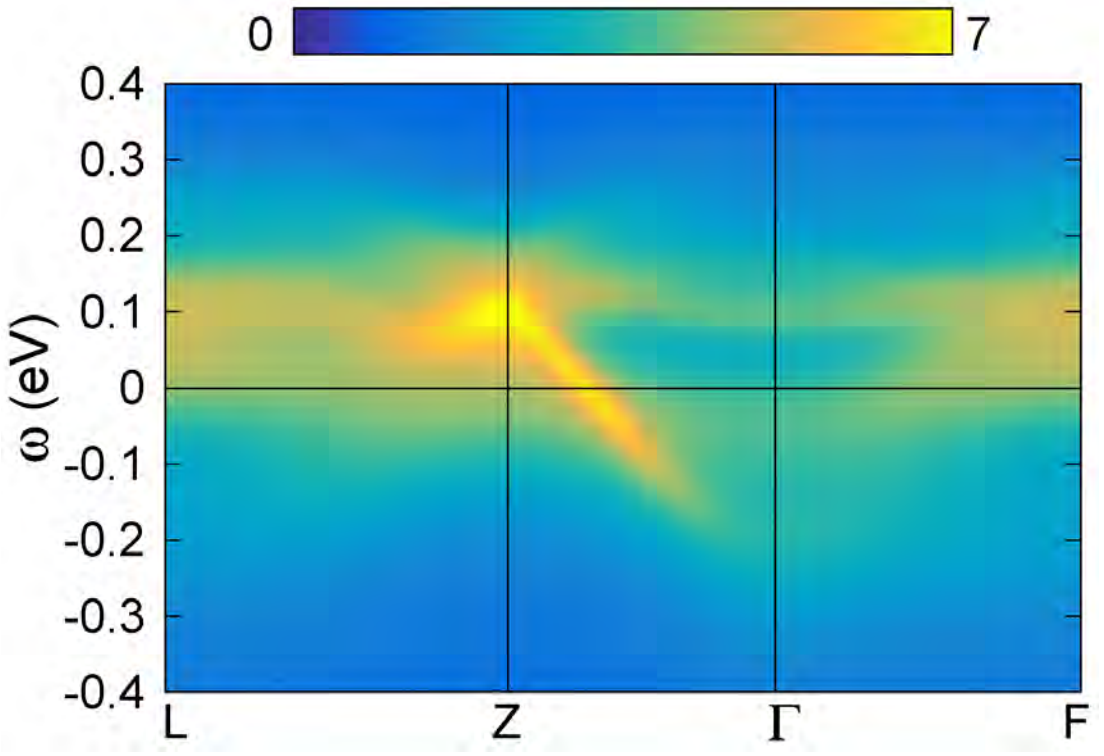

Fig. 6: *DFT+DMFT k-resolved spectral function $A(\mathbf{k},\omega)$ for stoichiometric V_2O_3 at $T = 193\,K$ along high-symmetry lines in the first Brillouin zone.*

its maxima. On the other hand, ρ_{bond} as a difference function has more contrast and reveals the charge redistributions due to the crystal environment. Here, one can see the charge transfer from V to O, especially originating from V-e_g. This is reasonable since V-e_g is strongly hybridized with O$(2p)$, which mainly responsible for the crystal bonding. The difference plot of $\rho_{\mathrm{diff}} = \rho_{\mathrm{DFT+DMFT}} - \rho_{\mathrm{DFT}}$ between DFT+DMFT and DFT in Fig. 7b verifies the already mentioned observation of enhanced V-e_g^{π} filling with correlations.

4.3 Charge self-consistency vs. one-shot

All the shown data corresponds to charge self-consistent DFT+DMFT. The relevance of charge self-consistency becomes already clear from our last finding of increased V-e_g^{π} filling with correlations. This increased filling affects the surrounding electronic structure and therefore has to be included on a complete self-consistent level.

However in V_2O_3, there are even much more dramatic consequences of charge self-consistency, which partly only become clear if one performs the same calculations at the simple one-shot level. If one does so, two major differences are observed. First, the orbital polarization already at stoichiometry is *much larger* [38,39] than with charge self-consistency [14,41–43,34], nearly close to fully polarized V-e_g^{π}. Hence the trend of trigonal-crystal-field enhancement due to correlations is artificially too strong because of the missing feedback of the rest of the system. This is verified by the recent ARPES measurements [44] at stoichiometry, which show a sizable a_{1g} occupation close to the finding with charge self-consistency. Second, and maybe even more relevant, the effective Cr-doped structure is already insulating in one-shot

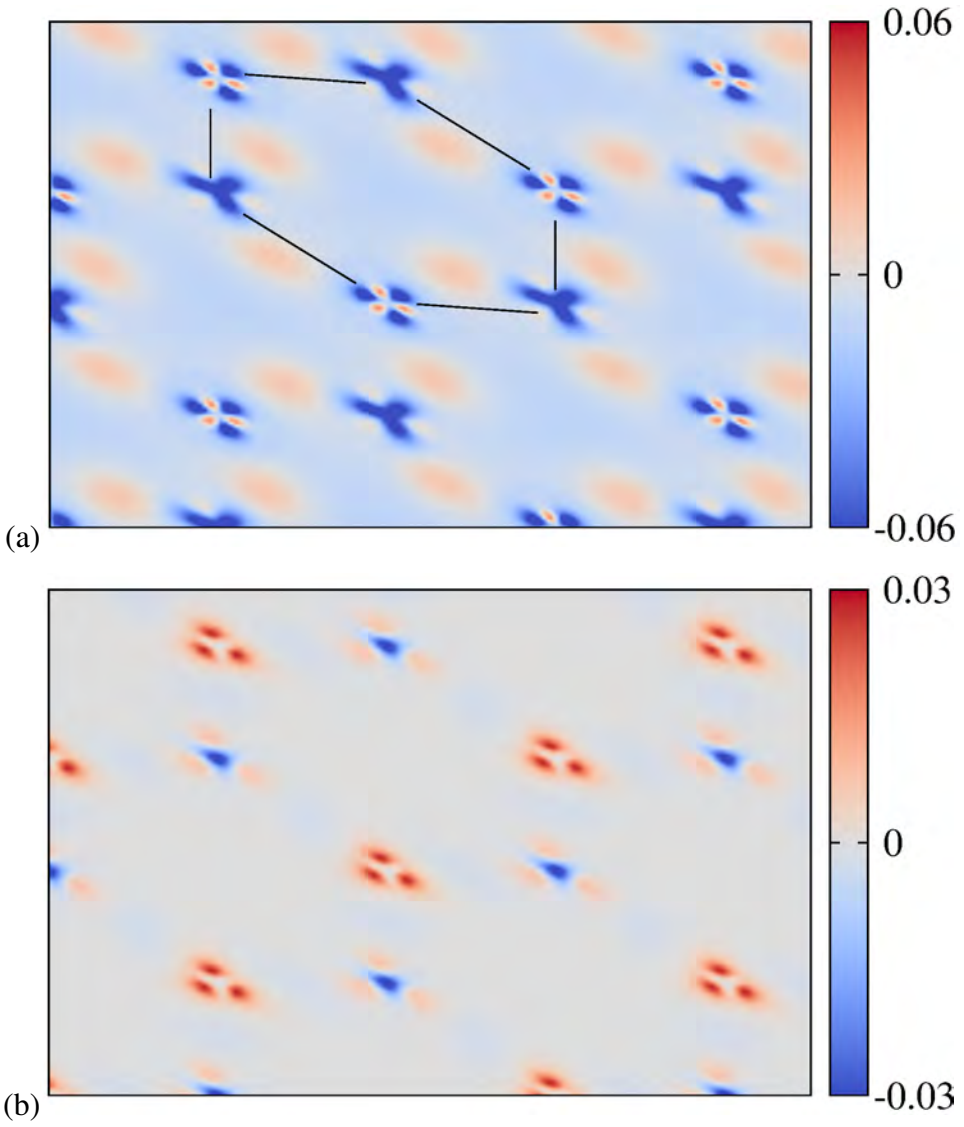

Fig. 7: *Inclined view on the charge density within the ab-plane of V_2O_3. (a) DFT+DMFT bonding charge density $\rho_{\mathrm{bond}} = \rho - \rho_{\mathrm{atomic}}$. Black lines are guides to the eye for the V-based honeycomb structure. Note that this is an effective honeycomb lattice, which is not exactly flat due two different height positions of V along c. (b) Charge-density difference $\rho_{\mathrm{diff}} = \rho_{\mathrm{DFT+DMFT}} - \rho_{\mathrm{DFT}}$ between DFT+DMFT and DFT. Note the enlarged occupation of the signatures of the V-e_g^π orbitals within DFT+DMFT (deep red parts).*

DFT+DMFT (e.g. Ref. [39]). Now one could say that is a good thing, because it matches with the phase diagram for that amount of doping. But one has to remember the strong simplifications that are used to arrive at that result: neglect of charge self-consistency as well as neglect of the explicit defect chemistry due to the Cr dopants. Thus, this "positive" result truly emerges from the (neglect-)error cancellation, and *does not* explain the true driving force behind the PM-PI transition.

In fact recent work [34] shows, that an honest treatment of *both* electronic correlations *and* explicit defect chemistry due to doping is relevant to understand the phase diagram of V_2O_3.

5 Concluding remarks

In this short lecture, we introduced the self-consistency cycles of different electronic structure approaches with an emphasis on charge self-consistency in DFT+DMFT. The interplay between the basic-formal schemes as well as rather technical-numerical aspects is of natural importance in this field. Furthermore, although the described methodologies and their concrete computer-code implementations are often very elaborate, one should never use them in a "black-box" manner. It remains very important as a physicist or materials scientist to interpret and weigh the obtained data, if possible by thoughtful consideration of experimental knowledge. Hence, true scientific results only appear after the numerical data is processed by a critical mind.

References

[1] N.W. Ashcroft and N.D. Mermin: *Solid State Physics* (Saunders College Publishing, 1976)

[2] R.O. Jones and O. Gunnarsson, Rev. Mod. Phys. **61**, 689 (1989)

[3] W. Kohn, Rev. Mod. Phys. **71**, 1253 (1999)

[4] W. Kohn and L.J. Sham, Phys. Rev. **140**, A1133 (1965)

[5] W. Metzner and D. Vollhardt, Phys. Rev. Lett. **62**, 324 (1989)

[6] A. Georges and G. Kotliar, Phys. Rev. B **45**, 6479 (1992)

[7] S.Y. Savrasov and G. Kotliar, Phys. Rev. B **69**, 245101 (2004)

[8] A. Georges: *in Lectures on the Physics of Highly Correlated Electron Systems VIII* (AIP Conference Proceedings 715, 2004), Ch. 3

[9] V.I. Anisimov, A.I. Poteryaev, M.A. Korotin, A.O. Anokhin, and G. Kotliar, J. Phys.: Condens. Matter **9**, 7359 (1997)

[10] A.I. Lichtenstein and M. Katsnelson, Phys. Rev. B **57**, 6884 (1998)

[11] S.Y. Savrasov, G. Kotliar, and E. Abrahams, Nature **410**, 793 (2001)

[12] J. Minár, L. Chioncel, A. Perlov, H. Ebert, M.I. Katsnelson, and A.I. Lichtenstein, Phys. Rev. B **72**, 045125 (2005)

[13] L.V. Pourovskii, B. Amadon, S. Biermann, and A. Georges, Phys. Rev. B **76**, 235101 (2007)

[14] D. Grieger, C. Piefke, O.E. Peil, and F. Lechermann, Phys. Rev. B **86**, 155121 (2012)

[15] F. Lechermann, A. Georges, A. Poteryaev, S. Biermann, M. Posternak, A. Yamasaki, and O.K. Andersen, Phys. Rev. B **74**, 125120 (2006)

[16] O.K. Andersen, Phys. Rev. B **12**, 3060 (1975)

[17] N. Marzari, A.A. Mostofi, J.R. Yates, I. Souza, and D. Vanderbilt, Rev. Mod. Phys. **84**, 1419 (2012)

[18] B. Amadon, F. Lechermann, A. Georges, F. Jollet, T.O. Wehling, and A.I. Lichtenstein, Phys. Rev. B **77**, 205112 (2008)

[19] V.I. Anisimov, D.E. Kondakov, A.V. Kozhevnikov, I.A. Nekrasov, Z.V. Pchelkina, J.W. Allen, S.-K. Mo, H.-D. Kim, P. Metcalf, S. Suga, A. Sekiyama, G. Keller, I. Leonov, X. Ren, and D. Vollhardt, Phys. Rev. B **71**, 125119 (2005)

[20] F. Lechermann: *Model Hamiltonians and Basic Techniques*,
in E. Pavarini, E. Koch, D. Vollhardt, and A. Lichtenstein (eds.):
The LDA+DMFT approach to strongly correlated materials
Modeling and Simulation, Vol. 1 (Forschungszentrum Jülich, 2011), Ch. 3

[21] E. Gull, A.J. Millis, A.I. Lichtenstein, A.N. Rubtsov, M. Troyer, and P. Werner,
Rev. Mod. Phys. **83**, 349 (2011)

[22] V.I. Anisimov, I.V. Solovyev, M.A. Korotin, M.T. Czyżyk, and G.A. Sawatzky,
Phys. Rev. B **48**, 16929 (1993)

[23] S. Biermann, F. Aryasetiawan, and A. Georges, Phys. Rev. Lett. **90**, 086402 (2003)

[24] M. Potthoff and W. Nolting, Phys. Rev. B **59**, 2549 (1999)

[25] M. Aichhorn, L. Pourovskii, and A. Georges, Phys. Rev. B **84**, 054529 (2011)

[26] D.B. McWhan, T.M. Rice, and J.B. Remeika, Phys. Rev. Lett. **23**, 1384 (1969)

[27] D.B. McWhan, J.B. Remeika, T.M. Rice, W.F. Brinkman, J.P. Maita, and A. Menth,
Phys. Rev. Lett. **27**, 941 (1971)

[28] C. Castellani, C.R. Natoli, and J. Ranninger, Phys. Rev. B **18**, 4945 (1978)

[29] L.F. Mattheiss, J. Phys.: Condens. Matter **6**, 6477 (1994)

[30] S.Y. Ezhov, V.I. Anisimov, D.I. Khomskii, and G.A. Sawatzky,
Phys. Rev. Lett. **83**, 4136 (1999)

[31] I.S. Elfimov, T. Saha-Dasgupta, and M.A. Korotin, Phys. Rev. B **68**, 113105 (2003)

[32] V. Eyert, U. Schwingenschlögl, and U. Eckern, Europhys. Lett. **70**, 782 (2005)

[33] Y. Guo, S.J. Clark, and J. Robertson, J. Chem. Phys. **140** (2014)

[34] F. Lechermann, N. Bernstein, I.I. Mazin, and R. Valentí, arXiv:1801.08906 (2018)

[35] P.D. Dernier, J. Phys. Chem. Solids **31**, 2569 (1970)

[36] S. Chen, J.E. Hahn, C.E. Rice, and W.R. Robinson, J. of Solid State Chem. **44**, 192 (1982)

[37] K. Held, G. Keller, V. Eyert, D. Vollhardt, and V.I. Anisimov,
Phys. Rev. Lett. **86**, 5345 (2001)

[38] G. Keller, K. Held, V. Eyert, D. Vollhardt, and V.I. Anisimov,
Phys. Rev. B **70**, 205116 (2004)

[39] A.I. Poteryaev, J.M. Tomczak, S. Biermann, A. Georges, A.I. Lichtenstein, A.N. Rubtsov,
T. Saha-Dasgupta, and O.K. Andersen, Phys. Rev. B **76**, 085127 (2007)

[40] M. Sandri, M. Capone, and M. Fabrizio, Phys. Rev. B **87**, 205108 (2013)

[41] D. Grieger and F. Lechermann, Phys. Rev. B **90**, 115115 (2014)

[42] X. Deng, A. Sternbach, K. Haule, D. Basov, and G. Kotliar,
Phys. Rev. Lett. **113**, 246404 (2014)

[43] I. Leonov, V.I. Anisimov, and D. Vollhardt, Phys. Rev. B **91**, 195115 (2015)

[44] I. Lo Vecchio, J.D. Denlinger, O. Krupin, B.J. Kim, P.A. Metcalf, S. Lupi, J.W. Allen, and A. Lanzara, Phys. Rev. Lett. **117**, 166401 (2016)